INTERNATIONAL JOURNAL FOR NUMERICAL METHODS IN FLUIDS, VOL. 6, 715–731 (1986)

NUMERICAL PREDICTIONS FOR UNSTEADY VISCOUS FLOW PAST AN ARRAY OF CYLINDERS

EDWARD A. CERUTTI,* ROBERT B. KINNEY† AND MICHAEL A. PAOLINO‡

Department of Mechanics, U.S. Military Academy, West Point, NY 10996, U.S.A.

SUMMARY

The unsteady two-dimensional flow around an array of circular cylinders submerged in a uniform onset flow is analysed. The fluid is taken to be viscous and incompressible. The array of cylinders consists of two horizontal rows extending to infinity in the upstream and downstream directions. The centre-to-centre distance between adjacent cylinders is fixed at three diameters, and the rows are staggered. Advantage is taken of spatially periodic boundary conditions in the flow direction. This reduces the computational domain to a rectangular region surrounding a single circular cylinder. Two cases, for Reynolds numbers of 1000 and 10,000, are presented.

KEYWORDS Viscous Flow Array of Cylinders Numerical Methods

INTRODUCTION

Numerical methods for predicting the two-dimensional viscous flow past single cylinders have received a great deal of attention in the past decade. The complex flow regimes associated with flow separation, wake development and vortex shedding can now be analysed with fast and novel finite-difference algorithms for Reynolds numbers of the order of one thousand.[1] The flows generated by single cylinders undergoing arbitrary accelerations can also be treated by rigorous means.[2]

When there are multiple bodies or arrays of bodies in the flow stream, the analysis becomes much more complicated. With one exception, all attempts to date have concentrated on solving the linearized equations which describe Stokes- and Oseen-type flows. Hasimoto[3] used periodic fundamental solutions to Stokes' equation to analyse the flow past a square array of circular cylinders. Happel[4] has studied the creeping motion past arrays of cylinders in order to model the flow through fibrous materials. More recently, two analytical studies[5,6] have been made of the slow viscous flow past pairs of cylinders, and experimental measurements[7] have been made of the frequency of vortex shedding behind two circular cylinders in a staggered arrangement. Except for

*Assistant Professor and Major.
†Visiting Professor and Professor, Aerospace and Mechanical Engineering Department, University of Arizona, Tucson, AZ 85721, U.S.A.
‡Professor and Colonel.

0271–2091/86/100715–17$08.50

Received 3 June 1985
Revised 10 March 1986

this latter study, the results of the aforementioned analyses are limited to Reynolds numbers less than 1·0.

One numerical study is known to the authors which treats the steady viscous flow through arrays of cylinders. Gordon[8] has used a vorticity–stream-function approach to calculate the steady flow field past various arrays placed transverse to a uniform stream. Unfortunately, this approach has a major deficiency, in that it is necessary to impose values for the vorticity and stream function at the boundary of the computational zone. When there is absolute flow symmetry, this presents no essential problem, since the lines of zero vorticity and constant stream function are straight and parallel to the onset flow, and they furthermore connect the centres of the cylinders. This is not the case when non-symmetrical vortex shedding destroys flow symmetry within an otherwise symmetrical arrangement of cylinders. In such cases, the locations and shapes of the contours of zero vorticity and constant stream function are not known *a priori*, and they furthermore do not coincide with simple co-ordinate surfaces.

A substantial problem was encountered by Gordon[8] when he tried to apply the standard techniques to compute the steady flow field past staggered arrays having several rows of cylinders. His iterative calculations did not converge, and although he attributed this to poor computer precision and the effect of round-off error on the calculation of the wall vorticity, it is suspected that the problem was due to the manner in which he arbitrarily enforced the flow boundary conditions. In any event, results were presented after 200 iterations for various configurations of cylinders for Reynolds numbers equal to 1 and 20.

Methods which do not incorporate the stream function do not have this limitation. For example, use can be made of the direct integral relationship between the velocity and vorticity fields (velocity induction law). This approach has already been used for a variety of flow problems by Kinney and his co-workers.[2,9–11] Wu has made a number of contributions to the integral formulation as well. These are summarized, discussed, and expanded upon in Reference 12.

The velocity induction law is a linear relationship which allows the velocity vector at any point in the flow to be computed from the superposition of vorticity fields throughout the flow regime. This is particularly useful if the flow is spatially periodic. The velocity field is then also spatially periodic, and no specific boundary values need be specified for the velocity components or the vorticity on the boundary of the computational domain. The flow is completely determined by the vorticity interior to the domain and the associated boundary condition imposed on its production at solid surfaces.

In the present study, we extend the aforementioned approach to predict numerically the unsteady two-dimensional flow past an array of cylinders. There are two rows in the array. Each row is infinitely long in the horizontal (flow) direction, and the cylinders are staggered. This basic arrangement differs from that studied by Gordon[8] in that the array is aligned with the flow direction rather than transverse to it.

Such an array of cylinders is found in many heat-exchanger applications. Each cylinder is in a non-uniform flow field, which is dominated by viscous effects associated with recirculating regions and wakes. Up to the present time, any knowledge about such flows has been gained through experimental measurements made on industrial-size equipment. This is the first attempt known to the authors to analyse the unsteady viscous flow through such arrays of cylinders at moderate Reynolds numbers.

ANALYSIS

The flow geometry is shown in Figure 1. The cylinders form two horizontal rows, which are infinitely long and staggered. Fluid extends to infinity above and below the rows. Each cluster of

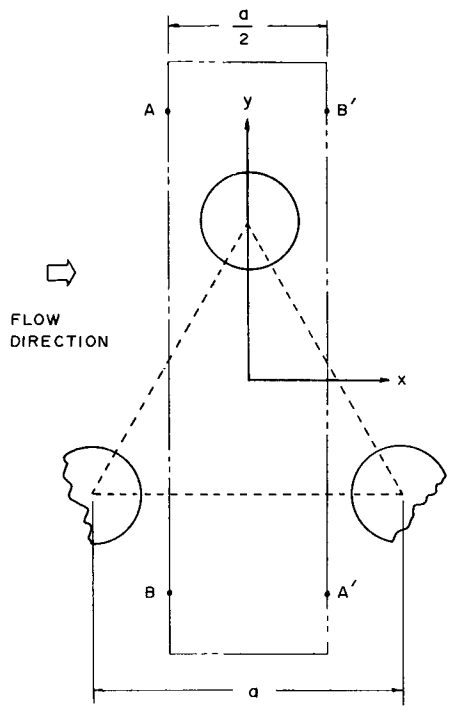

Figure 1. Flow geometry with primary computational region shown

three cylinders forms an equilateral triangle, and the centre-to-centre distance between two cylinders along one side of the triangle is three cylinder diameters.

The flow is started impulsively from rest with uniform velocity, U_∞. The flow is in the horizontal direction and may be visualized as being from left to right. The initial condition is that corresponding to inviscid flow past the array of cylinders. At each time level, the no-penetration condition is enforced by distributing bound vorticity on the cylinder surfaces. The enforcement of the viscous adherence condition causes free vorticity to be produced at the cylinder surfaces. This free vorticity enters the exterior flow and, as time progresses, it forms the boundary-layer and wake regions behind the cylinders.

Since the cylinders are arranged with uniforms spacing in the horizontal direction, it is reasonable to expect that the flow will be spatially periodic. That is, the same flow picture should be produced if one shifts the field of view any arbitrary number of cylinders to the right or to the left. Furthermore, it is apparent that the same arrangement of cylinders is produced if the array is rotated 180° about one of the cylinders. Since the direction of flow is arbitrary, the flow picture should thus be invariant to such a rotation and a reversal in the flow direction. This implies that there should be staggered antisymmetry with respect to a horizontal plane situated midway between the rows.

Governing equations

Under the aforementioned idealizations, it is only necessary to analyse the flow in a domain of width equal to one-half the spatial period (i.e. $a/2$) and centred on a single cylinder. This domain is rectangular in shape and is shown by the dashed boundary in Figure 1. The

antisymmetry is enforced at the vertical boundaries of the domain. Corresponding antisymmetric points are shown on the vertical right- and left-hand boundaries. These are A–A′ and B–B′, respectively.

At any given time level, the free vorticity which may leave the domain at point A′, say, is assumed to enter the domain at point A with equal strength but opposite sign (sense of rotation). The same is true for points B′ and B. It is further assumed that the top and bottom horizontal boundaries of the flow domain are sufficiently far from the cylinders that free vorticity does not cross them. The flow field need not be uniform there with velocity U_∞, but it is assumed to be irrotational so that the free vorticity is zero above and below the horizontal boundaries of the computational domain.

The zero penetration condition on the flow at the cylinders is enforced by distributing bound vorticity, γ, on their surfaces. This 'bound' vorticity is not to be confused with 'boundary' vorticity. The latter is associated with the free vorticity, ω. Boundary vorticity is not used here. Rather, the local production of free vorticity at the cylinders is found from the enforcement of the viscous adherence condition. This is discussed at a later point in the analysis (see equation (10)).

The velocity induction law gives the velocity at any point p in the flow in terms of integrals of the free and bound vorticities, plus the uniform onset flow velocity, U_∞. The law can be expressed in terms of the rectangular co-ordinates shown in Figure 1. The y-axis goes through the centre of the cylinder and the x-axis is midway between the two horizontal rows of cylinders. Thus one has

$$\mathbf{V}_p = U_\infty \mathbf{i} + \sum_{n=-\infty}^{+\infty} \left[\frac{1}{2\pi} \int\int_A \frac{\boldsymbol{\omega}_0^n \times \mathbf{r}_{0p}^n}{(r_{0p}^n)^2} \mathrm{d}A_0 + \frac{1}{2\pi} \int_C \frac{\boldsymbol{\gamma}_s^n \times \mathbf{r}_{sp}^n}{(r_{sp}^n)^2} \mathrm{d}l \right]. \tag{1}$$

An element of free vorticity is located at point 0 in the fluid, and an element of bound vorticity is located at point s on a cylinder of circumference C. The area of integration, A, is over the computational domain. The superscript n denotes that a summation must be made over the infinite number of periodically repeating regions located to the left and right of the computational domain.

For this two-dimensional flow, $\boldsymbol{\omega} = \omega \mathbf{k}$ and $\boldsymbol{\gamma} = \gamma \mathbf{k}$. We are interested first in evaluating only the x-component of velocity from (1). The integration and summation operations can be interchanged, so that it is required to evaluate an infinite series of the form

$$\sum_{n=-\infty}^{+\infty} \frac{\mathbf{k} \times \mathbf{r}_{0p}^n}{(r_{0p}^n)^2} \cdot \mathbf{i} = -\frac{y}{y^2 + x^2} - \sum_{n=1}^{\infty} \left[\frac{y}{y^2 + (x - na)^2} + \frac{y}{y^2 + (x + na)^2} \right]. \tag{2}$$

For notational simplicity, the vortex element has been assumed to be at the origin of co-ordinates, and the point p is at (x, y). The first term in the foregoing represents the contribution to the geometrical kernel from the vorticity in the computational zone. The remaining terms arise as we repeat this vorticity for n regions to the right and left. Here a is the spatial period, which is equal to 3 cylinder diameters. We have not yet introduced staggered antisymmetry into the expression.

It is recognized that the series given in (2) also arises in the potential-flow theory used to describe a von Karman vortex street. It is evaluated in closed form by Milne-Thomson,[13] and a detailed development is given in the dissertation[14] on which this paper is based. When the result is expressed for the vortex element located at a general point in the upper half-plane, one has

$$\sum_{n=-\infty}^{+\infty} \frac{\mathbf{k} \times \mathbf{r}_{0p}^n}{(r_{0p}^n)^2} \cdot \mathbf{i} = -\frac{\pi}{a} \left[\frac{\sinh \frac{2\pi}{a}(y_p - y_0)}{\cosh \frac{2\pi}{a}(y_p - y_0) - \cos \frac{2\pi}{a}(x_p - x_0)} \right]. \tag{3}$$

The expression given by (3) is rigorously valid for a vortex element in the upper half plane of Figure 1. To generalize it to any vortex element in the computational domain, we use the assumption that the vorticity field is staggered antisymmetrically with respect to the x-axis. Thus we must introduce another term into (3), which corresponds to the image vortex element of opposite sense of rotation (negative sign) and located at the point with co-ordinates x' and y', where $y' = -y$ and $x' = -a/2 + x$. The term $-a/2$ reflects the fact that the lower row of cylinders is staggered an amount $a/2$ relative to the top row. The final result for the x-component of the first integral in (1) can be written

$$\sum_{n=-\infty}^{+\infty} \frac{1}{2\pi} \iint_A \frac{\boldsymbol{\omega}_0^n \times \mathbf{r}_{0p}^n}{(r_{0p}^n)^2} \cdot \mathbf{i}\, dA_0 = -\frac{1}{2a} \iint \left[\frac{\sinh \frac{2\pi}{a}(y_p - y_0)}{\cosh \frac{2\pi}{a}(y_p - y_0) - \cos \frac{2\pi}{a}(x_p - x_0)} - \frac{\sinh \frac{2\pi}{a}(y_p + y_0)}{\cosh \frac{2\pi}{a}(y_p + y_0) + \cos \frac{2\pi}{a}(x_p - x_0)} \right] \omega_0 \, dx_0 \, dy_0. \tag{4}$$

In the foregoing, use has been made of the fact that $\cos 2\pi(x_p - x_0')/a = -\cos 2\pi(x_p - x_0)/a$.

A similar expression can be developed for the x-component of the second integral in (1), which involves the bound vorticity, γ. All that is needed is to change the subscript 0 in (4) to s, and note that the integral is over the cylinder contour with arc length dl.

To summarize, the general velocity vector, $\mathbf{V}_p$, is given by (1). The x-component of this velocity involves the expression given in (4) plus its counterpart involving the bound vorticity. An expression for the y-component can be obtained in an analogous fashion, and the result is

$$\sum_{n=-\infty}^{+\infty} \frac{1}{2\pi} \iint_A \frac{\boldsymbol{\omega}_0^n \times \mathbf{r}_{0p}^n}{(r_{0p}^n)^2} \cdot \mathbf{j}\, dA_0 = \frac{1}{2a} \iint \left[\frac{\sin \frac{2\pi}{a}(x_p - x_0)}{\cosh \frac{2\pi}{a}(y_p - y_0) - \cos \frac{2\pi}{a}(x_p - x_0)} + \frac{\sin \frac{2\pi}{a}(x_p - x_0)}{\cosh \frac{2\pi}{a}(y_p + y_0) + \cos \frac{2\pi}{a}(x_p - x_0)} \right] \omega_0 \, dx_0 \, dy_0, \tag{5}$$

where only the result for the first integral in (1) has been written out explicitly. The expression for the y-component of the second integral in (1) is obtained in a similar fashion. Once the two Cartesian components of the velocity vector are known, the component in any arbitrary direction can be determined.

Note that the velocity terms are given by closed-form expressions. That is, no series summations are required. Also it follows that since the bound and free vorticities are spatially periodic, so too will be the velocity field.

The next step is to develop the integral equation for the bound vorticity. This is obtained by specializing equation (1) for a point p just interior to the cylinder surface. The velocity component tangential to the cylinder is taken, and this velocity is equated to zero. Note is made of the fact that γ represents a discontinuity in the tangential component of velocity across the cylinder surface (zero interior to the cylinder and $-\gamma$ on the surface). The final governing equation

for γ is obtained as follows:

$$\gamma(\phi) - \frac{1}{2a}\int_0^{2\pi} K(\theta, y_p, y_q, x_p, y_q)\gamma(\theta)\mathrm{d}\theta = -2[u_w(\phi) + \sin\phi], \tag{6}$$

where a cylindrical polar co-ordinate system has been adopted since all the bound vorticity is on the surfaces of the cylinders.

In the foregoing, the angles are measured in the counter-clockwise direction from the rear (i.e. downstream) stagnation point of the cylinder towards the front. The angle ϕ gives the location of the point p where the tangential velocity component is evaluated. The angle θ gives the location of any other bound vortex point q. Thus

$$\begin{aligned} y_p &= 0{\cdot}5\sin\phi, \quad y_q = 0{\cdot}5\sin\theta, \\ x_p &= 0{\cdot}5\cos\phi, \quad x_q = 0{\cdot}5\cos\theta, \end{aligned} \tag{7}$$

and the cylinder radius has been set equal to 0·5. Also, the variables have been non-dimensionalized with respect to the free-stream velocity, U_∞. The geometrical kernel in (5) is given by

$$K(\theta, x_p, y_p, x_q, y_q) = \left[\frac{\sin\theta\sinh\frac{2\pi}{a}(y_p - y_q) + \cos\theta\sin\frac{2\pi}{a}(x_p - x_q)}{\cosh\frac{2\pi}{a}(y_p - y_q) - \cos\frac{2\pi}{a}(x_p - x_q)} - \frac{\sin\theta\sinh\frac{2\pi}{a}(y_p + y_q) - \cos\theta\sin\frac{2\pi}{a}(x_p - x_q)}{\cosh\frac{2\pi}{a}(y_p + y_q) + \cos\frac{2\pi}{a}(x_p - x_q)}\right]. \tag{8}$$

The quantity $u_w(\phi)$ in the non-homogeneous term of (6) is the tangential component of velocity induced at the cylinder by the free vorticity in the fluid. It is given by

$$u_w(\phi) = \frac{1}{2a}\int\int_A K(\phi, x_p, y_p, x_0, y_0)\omega_0\,\mathrm{d}A_0, \tag{9}$$

where x_p and y_p are as given in (7), and x_0, y_0 denote the co-ordinates of the free vortex element, ω_0. Except for the different kernel functions, equation (6) is identical to that used in Reference 2.

The bound vorticity, γ, obtained from equation (6) represents an apparent slip velocity on the surface of the cylinder. Following the methods of References 2 and 9–11, the slip velocity must be reduced to zero by the proper production of free vorticity at the cylinder surface over a suitable time increment. This couples the bound vorticity to the free vorticity through the boundary condition imposed on the solution for the free vorticity. In dimensionless form, the boundary condition in cylindrical polar co-ordinates is

$$-\frac{1}{Re}\int_t^{t+\Delta t}\left(\frac{\partial\omega}{\partial r}\right)_{r=0{\cdot}5}\mathrm{d}t = \gamma(t). \tag{10}$$

The solution of the governing equation for γ and the calculation of the velocity and free vorticity fields were carried out numerically. This is discussed in the next section.

Numerical formulation

The first task was to develop a suitable grid for the computational zone surrounding the cylinder. The cylinder of unit diameter was first circumscribed by two concentric circles of radii

$0{\cdot}5 + \Delta r_1$ and $0{\cdot}5 + \Delta r_2$. These circles formed the boundaries of two uniform layers of cells adjacent to the cylinder. Between the second concentric circle and the rectangular outer boundary of the computational region, a non-orthogonal grid was generated using the method of Thames.[15] A flow network of 80×29 fluid cells was generated, as shown in Figure 2. There are eighty cells of equal width $0{\cdot}5\,\Delta\theta$ spaced around the circumference of the cylinder. The cells lines $\xi = \text{constant}$ emanate from the cylinder radially and eventually intersect the outer rectangular boundary. The first of the closed curves $\eta = \text{constant}$ is that of the cylinder surface. These curves are numbered sequentially in the radial direction, with the final curve coinciding with the rectangular outer boundary of the computational region. This non-orthogonal grid has the advantage that the lines of $\xi = \text{constant}$ in the central (i.e. primary) computational zone match up with those in the inverted 'mirror image' zones to the right and left at the mutual boundaries. Also there is good flow resolution near the surfaces of the cylinders.

The network generated by the method of Thames[15] produced the co-ordinates in the x–y plane of the intersection of the curves $\eta = \text{constant}$ and $\xi = \text{constant}$. These intersection points were connected with straight-line segments, thus producing fluid cells which are quadrilaterals. The direction normal to each side was determined by analytical geometry, as were the lengths of the sides and the areas of each cell.

A typical fluid cell is shown in Figure 3. Velocity components were first obtained at the centre points of each side $\xi = \text{constant}$ in the direction of the inward and outward drawn normals to the sides. This required numerical evaluations of the integrals in equations (4) and (5), plus those involving the bound vorticity. Once the two Cartesian components, of the velocity were found, they were resolved along the normal directions to the cell boundaries to give u_1 and u_2, as

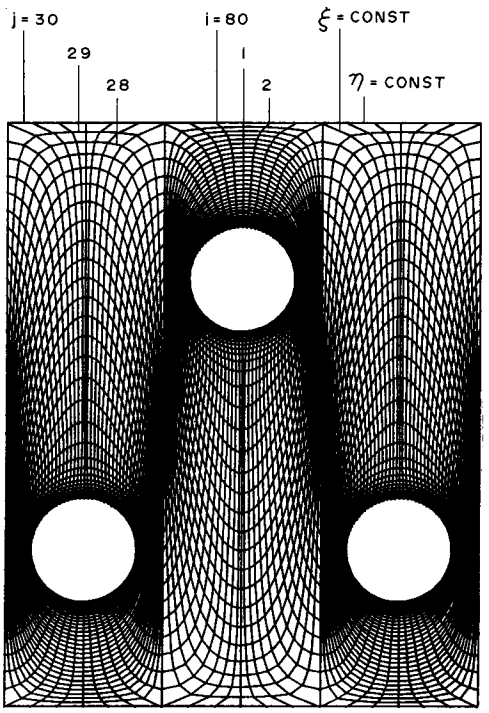

Figure 2. Flow network employed in numerical formulation

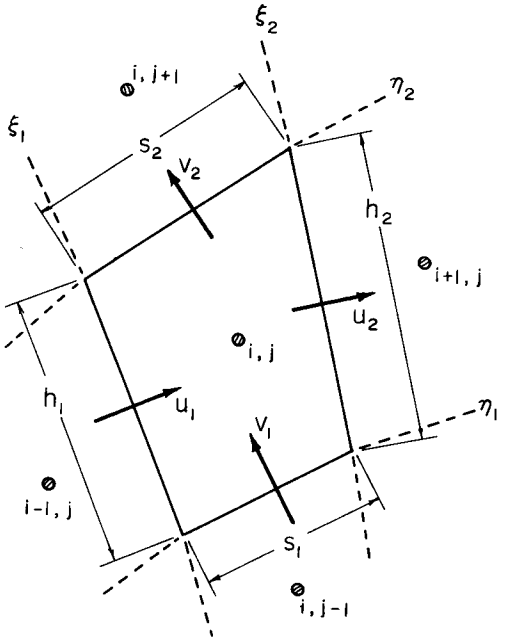

Figure 3. Schematic diagram of a typical fluid element interior to the flow

shown in Figure 3. The integration procedure is described more fully in the subsequent paragraphs. The velocity components in the direction normal to the sides with $\eta = \text{constant}$ were obtained by enforcing the principle of mass conservation. The process began with the fluid cells next to the cylinder, where the velocity normal to the cylinder was known to be zero.

Consider, for example, some interior cell. By the aforementioned procedure, the velocity at the bottom of the control volume (i.e. v_1) plus those on the sides, u_1 and u_2 are known; then v_2 needed to satisfy mass conservation is given by

$$v_2 = v_1 \frac{s_1}{s_2} + \frac{1}{s_2}(u_1 h_1 - u_2 h_2). \tag{11}$$

For a selected point (x_p, y_p), the integrations shown in (4) and (5) were performed over each fluid cell in the mesh, assuming that the vorticity in each cell was uniform. The assumption that γ was uniform over each surface segment of length $0{\cdot}5\Delta\theta$ was also made for corresponding integrations involving the bonund vorticity. For the most part, the vortex elements were sufficiently far from the point p that each element could be treated as a point vortex of strength $\omega_0 \Delta A_0$ or $0{\cdot}5\gamma_s \Delta\theta$, located at the centroids of the cell or surface segment. These were then multiplied by the terms in brackets in (4) and (5).

The point-vortex approximation was not used when the distance between the element centre and the point p was less than 5 times the largest diagonal dimension of the element. In those cases, the quantity in brackets in (4) and (5) had to be integrated over the region of interest, but the vortex strengths were still assumed to be uniform.

The procedure involved first evaluating the Cartesian velocity components using the point vortex approximation throughout. Call this result $\Delta u'_p$, say. The exact form for this velocity

due to the free vorticity was then calculated from the expression

$$\Delta u_p = \Delta u'_p - \frac{\omega_0 \Delta A_0}{2\pi}\left[-\frac{(y_p - y_0)}{(y_p - y_0)^2 + (x_p - x_0)^2}\right] + \frac{\omega_0}{2\pi}\iint_{\Delta A_0}\left[-\frac{(y_p - y_0)}{(y_p - y_0)^2 + (x_p - x_0)^2}\,dx_0 dy_0\right]. \quad (12)$$

In this way, the contribution due to the (assumed) point vortex located at point 0 was subtracted out of the expression, and the more exact integrated result was added in.

The integral in the above was evaluated following the same procedure used in Reference 2. That is, the integration can be performed exactly with respect to y_0 for a differential strip of width dx_0. The final integration with respect to x_0 was performed numerically using a 40-point Gauss–Legendre quadrature formula. For the integration over a surface segment of a cylinder, the 40-point quadrature formula was also used.

Regardless of whether the point-vortex approximation or the more exact numerical quadrature procedures were used, the end result was a vorticity magnitude (either bound or free) multiplied by a geometrical coefficient. To aid the numerical evaluations of the velocity at each point p, the geometrical coefficients for each cell and each surface segment were generated once and then stored on magnetic disk. They were then retrieved and used as needed in the flow calculations.

The principle of the conservation of vorticity was also applied to each fluid cell. This required the evaluation of the transport of vorticity (by diffusion and convection) across the cell boundaries. The vorticity convected across a cell boundary was taken to be that from the upwind cell. For example, the vorticity convected across the surface ξ_1 in Figure 3 by velocity u_1 was set equal to that at node $(i-1,j)$. Diffusion was evaluated centrally by computing the flux based on the vorticity difference between node points in adjacent cells divided by the separation distance between cell centroids. The (Euler) explicit time method was used to evaluate the time rate of change of the free vorticity in a given cell. That is, the rate of convective and diffusive transport of vorticity into the cell centred upon node (i,j) was assumed to take place at time t. The time rate of change of vorticity in the cell was then given by

$$\Delta A_{i,j}[\omega_{i,j}(t + \Delta t) - \omega_{i,j}(t)]/\Delta t.$$

The pressure distribution around the cylinder, the wall shear stress, and the associated lift, drag and moment coefficients were evaluated using a procedure identical to that in Reference 2.

RESULTS AND DISCUSSION

It is realized that the underlying assumption that the flow is spatially periodic and has staggered antisymmetry may not be realistic for flows at moderate to high Reynolds numbers. It certainly implies a geometrically perfect array and the absence of external disturbances. As the Reynolds number increases, the flow could become unstable to even small disturbances. However, it is not yet known when such effects could occur, or even if they are significant. By computing the unsteady (but nevertheless two-dimensional) flow using the full vorticity transport equation, we do allow for the growth of non-linear but spatially periodic disturbances, such as those introduced by non-symmetrical vortex shedding from the cylinders. Other effects cannot be accounted for by the present analysis.

Numerical calculations have been carried out for an array of cylinders with Reynolds numbers of 100, 1000 and 10,000. Only the results for the higher two Reynolds numbers are presented here. Campanion calculations have been carried out for a single cylinder in cross flow at the same

Reynolds numbers. The results of the latter calculations have been compared with those from other studies of the steady and unsteady flow over a single cylinder.

The single cylinder was located at the centre of a square computational region. The non-orthogonal (but nevertheless symmetrical) grid was generated using the method of Thames,[15] with 80 grid increments in the circumferential direction around the cylinder and 40 grid increments between the cylindrical surface and the square outer boundary of the computational domain. The length of this boundary was varied from three to eighteen cylinder diameters with minor changes in the outcome of the results. Steady state values for the drag coefficient compared very favourable with studies performed by Thoman and Szewczyk,[16] Jordan and Fromm,[17] Chorin,[18] Gollins and Dennis[19] and Fornberg.[20]

Unsteady numerical results obtained with the 3×3 computational domain were compared with those from a previous analytical study[21] at a Reynolds number of 1000. It was found that at $t = 0{\cdot}75$, the wall-shear stress distributions computed by the two methods agreed very well up to the vicinity of the sparation point. Beyond that point, the analytical results showed a stronger reverse flow than that found in the numerical calculations. However, the results were inconclusive in this region because insufficient terms were carried in the series expansion to allow the shear stress to be evaluated over the entire surface in the backflow region. Also, the flow is very sensitive to the pressure distribution here, and the Blasius expansion begins to lose validity as the wake and region of separated flow grow with time. Therefore, it is felt that the comparisons are satisfactory for our purposes.

The results to be emphasized here are for the array of cylinders. The dimensionless time step (based on diameter) was $\Delta t = 0{\cdot}008$ for both Reynolds numbers. The two layers of cells next to the surfaces of each cylinder had equal radial increments of 0·016 diameters. It is realized that maintaining the same cell sizes for the higher Reynolds number introduces some additional artificial viscosity into the results. However, it was not feasible to decrease the cell size, since the concomitant increase in the number of cells, and thus the geometrical coefficients, would cause the execution time to exceed practical limits. The calculations were carried out at the higher Reynolds number in order to demonstrate that the numerical techniques employed in this study are suitable for moderate Reynolds numbers, and to show the general trends of the results at this higher Reynolds number.

The time development of the viscous regions near the cylinders for a Reynolds number of 1000 can be followed in Figure 4. Contours of constant vorticity are shown at early, intermediate, and advanced time levels. Note that corresponding contours for the lower row of cylinders have signs opposite to those for the upper row of cylinders. At $t = 0{\cdot}75$, it is noteworthy that the line of zero vorticity links the forward and rear stagnation points of cylinders in adjacent rows. After the passage of 3·75 dimensionless time units, the wake behind each cylinder is quite asymmetrical, and three contours of the zero vorticity have emerged. Two link the cylinders in each row, and one forms a continuous curve throughout the region of fluid between the two rows of cylinders. It can be seen that negative vorticity is just beginning to break away from the outside surfaces of the upper and lower cylinders. The process is more complete for $t = 5{\cdot}75$, which is slightly less than the last time for which results have been computed, $t = 6{\cdot}0$. Note that no problem arises due to the convection of vorticity beyond the computational zone in the downstream direction, since the flow domain has effectively been extended to infinity by the use of a spatially periodic region of flow. It is felt that the major flow development has occurred by the time a particle moving with the undisturbed stream has traveled 6 cylinder diameters, which is equivalent to 6 units of dimensional time.

It is important to note that the contours of zero vorticity in Figure 4 are not straight, nor do they coincide with co-ordinate lines. This follows since there is no symmetry inherent to the flow. Thus

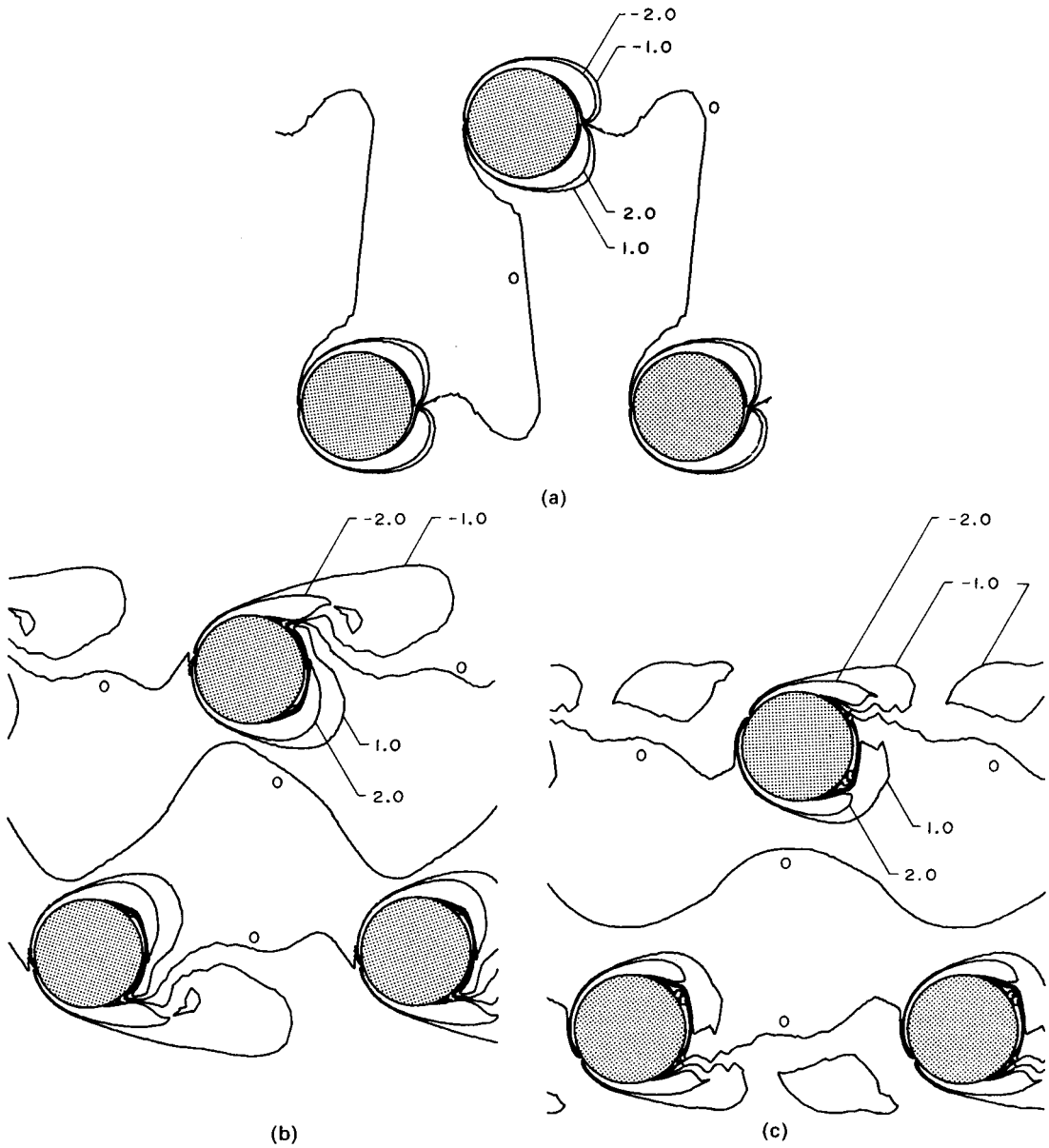

Figure 4. Time development of vorticity contours for $Re = 1000$: (a) $t = 0{\cdot}75$; (b) $t = 3{\cdot}75$; $t = 5{\cdot}75$

the conventional stream-function – vorticity formulation used by Gordon[8] cannot be applied to this flow problem.

An indication of the velocity distributions on the outer boundary of the computational region for a Reynolds number of 1000 is shown in Figure 5. Here, velocity vectors depicting the horizontal velocity component are shown on the vertical portions of the domain. The vector just below the central diagram represents the magnitude of the undisturbed free stream velocity. The vertical velocity components on the upper and lower portions of the diagram have been magnified by a factor of ten in order to make them show up more clearly.

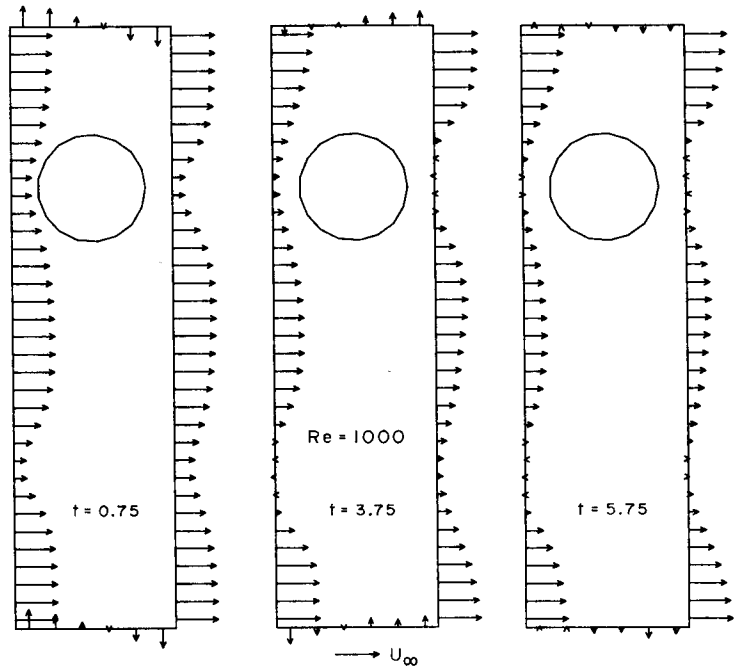

Figure 5. Velocity profiles on the boundary of the computational region at various times: $Re = 1000$

It can be seen from Figure 5 that there is flow reversal behind the cylinders for $t = 3{\cdot}75$ and $t = 5{\cdot}75$. Also there is a small amount of flow transverse to the cylinders across the upper and lower horizontal boundaries. This is not suppressed in the current calculations and is allowed to occur naturally. It is assumed that the free vorticity of the fluid is zero beyond the upper and lower boundaries. Therefore, no vorticity is allowed to enter the computational domain across these boundaries by convection. There is a small amount of convective and diffusive transport out of the domain, however.

The development of the drag coefficient with time for a Reynolds number of 1000 is shown in Figure 6. The general behaviour is shown to be initially similar to that for flow over a single cylinder. As time progresses, however, the drag coefficient for a cylinder in the array is seen to drop continuously and appears to be approaching an asymptotic value.

Figure 7 demonstrates the development of the lift coefficient with time. Note that it generally carries a negative sign and exhibits a cyclical behaviour. A negative lift coefficient indicates that the cylinder rows are experiencing forces which attempt to drive them towards each other.

The time development of the constant vorticity contours for a Reynolds number of 10,000 are shown in Figure 8. The calculations at this higher Reynolds number were carried out to 14·5 dimensionless time units. The flow develops in a manner similar to that for a Reynolds number of 1000. Note once again that after the passage of 3·75 dimensionless time units, the zero vorticity contours form a continuous curve between cylinders in the same row.

The development of the drag coefficient with time for a Reynolds number of 10000 is shown in Figure 9. Note that the drag curve generally decreases with time and does not achieve a relatively steady value, as it does in the case of a single cylinder. Also it would be erroneous to conclude that the curve had flattened out at a dimensionless time of approximately 5·5. This indicates that the results for the case of $Re = 1000$ most probably are not at steady state for $t = 6{\cdot}0$.

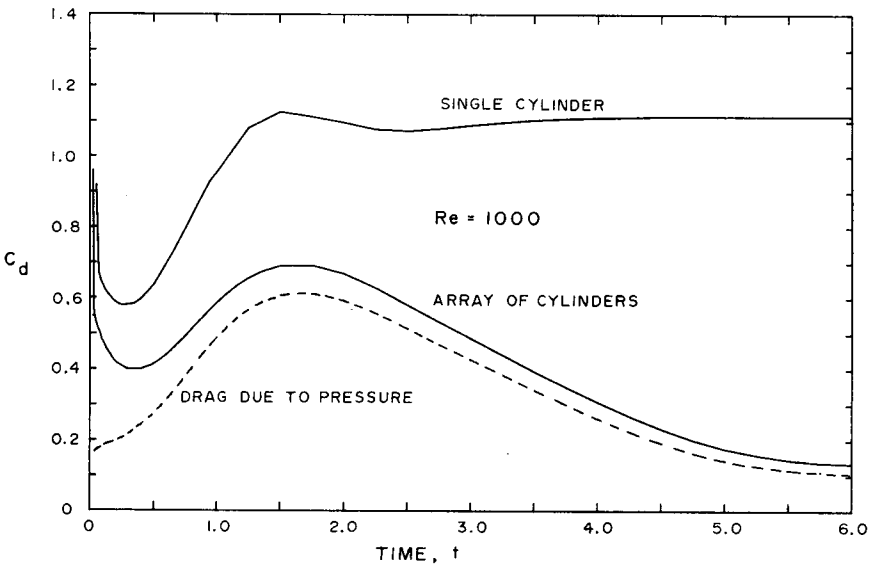

Figure 6. Time variation of drag coefficient for flow over a single cylinder and the array of cylinders: $Re = 1000$

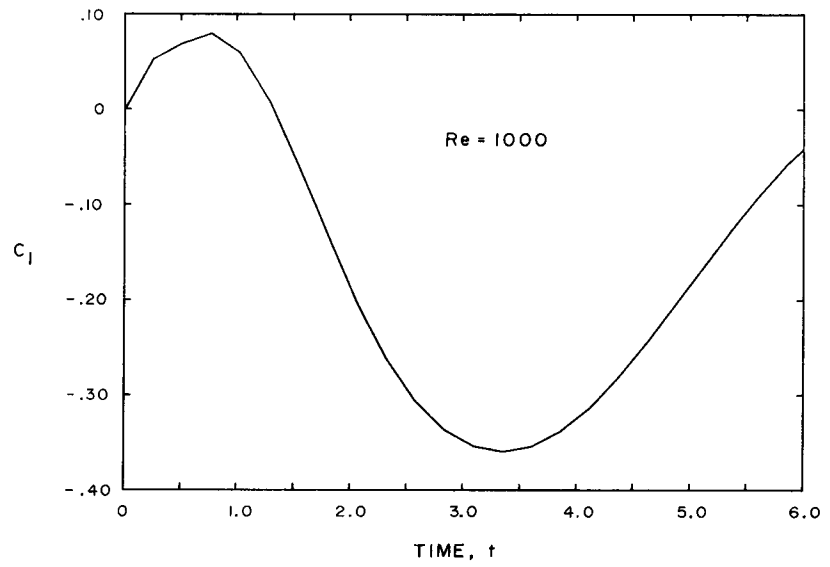

Figure 7. Time variation of lift coefficient for flow over the array of cylinders: $Re = 1000$

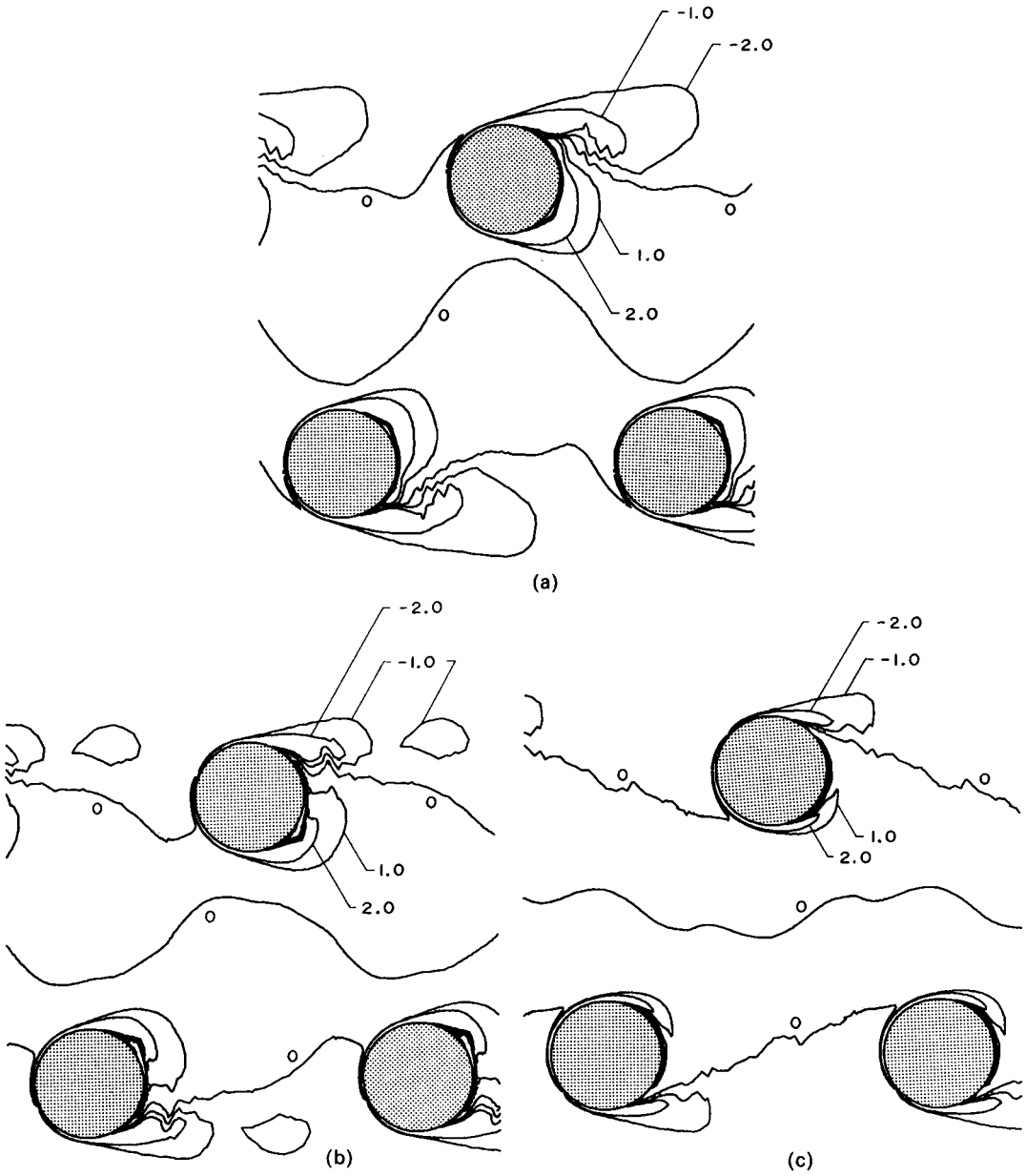

Figure 8. Time development of vorticity contours for $Re = 10{,}000$: (a) $t = 3{\cdot}75$; (b) $t = 5{\cdot}75$; (c) $t = 14{\cdot}5$

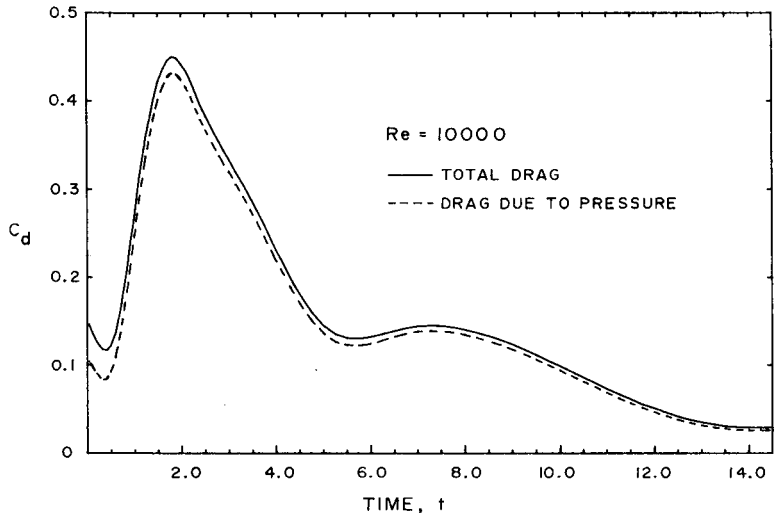

Figure 9. Time variation of drag coefficient for flow over the array of cylinders: $Re = 10{,}000$

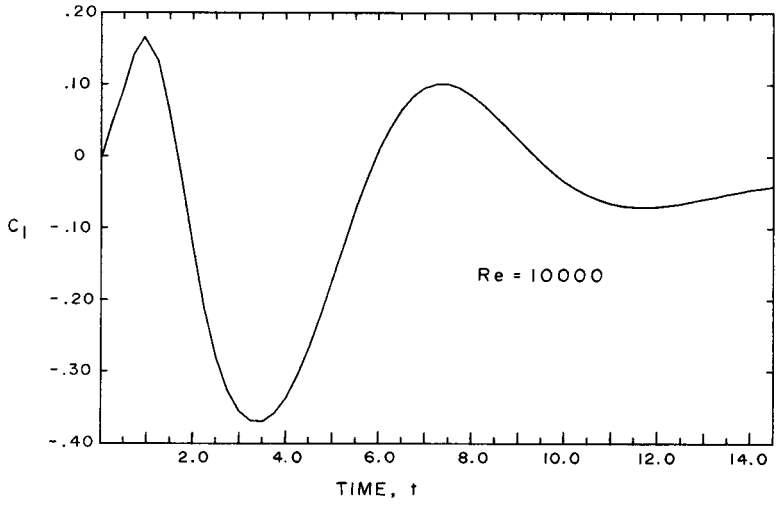

Figure 10. Time variation of lift coefficient for flow over the array of cylinders: $Re = 10{,}000$

Figure 10 demonstrates the development of the lift coefficient with time for $Re = 10{,}000$. Note once again the cyclical behaviour of the curve. In this case, however, the amplitude of the oscillations appears to be damping out with time. Also, the lift coefficient is positive between $t = 6{\cdot}0$ and 9·3. During this time the fluid forces are tending to separate the cylinders.

CONCLUDING REMARKS

The two-dimensional analysis of the unsteady viscous flow past an array of cylinders has been developed from basic kinematical and dynamical principles. The approach used in the present study is an extension of that applied to single cylinders.[2,10]

We have demonstrated that the method is amenable to flows which are spatially periodic. Determination of the velocity field from the velocity induction law then involves the evaluation of an infinite series, which may be expressed in closed form using classical results given by Milne-Thomson.[13]

The principal advantage of the current method is that the stream function does not appear in the formulation, and thus values for this quantity need not be specified on the boundaries of the computational domain. Furthermore, lines of zero vorticity (i.e. flow symmetry) need not be specified. This is in sharp contrast to the conventional approach used by Gordon,[8] which breaks down whenever steady symmetrical flows do not occur for the prescribed Reynolds number. The authors believe that this was the probable cause of the convergence difficulties encountered by Gordon[8] for the staggered array of cylinders, and not the lack of computational precision, as hypothesized by him.

ACKNOWLEDGEMENTS

The authors express their appreciation to the U. S. Military Academy for providing accesss to a PRIME 850 computer on which this work was performed.

NOMENCLATURE

a	Spatial period. Distance between adjacent cylinders on the same horizontal row.
A	Area of integration.
C	Circumference of cylinder.
C_d	Drag coefficient (Drag/$0{\cdot}5\rho U_\infty^2 D$)
C_l	Lift coefficient (Lift/$0{\cdot}5\rho U_\infty^2 D$)
D	Cylinder diameter
h_1, h_2	Lengths of the side of a control volume (see Figure 3)
$\mathbf{i}, \mathbf{j}, \mathbf{k}$	Unit vectors in the x, y and z directions.
K	Geometrical kernel function defined in equations (8) and (9).
l	Length of element on cylinder surface.
$\mathbf{r}$	Position vector.
$\mathbf{r}_{0p}$	$\mathbf{r}_p - \mathbf{r}_0$
Re	Reynolds number ($U_\infty D/\nu$)
s_1, s_2	Lengths of the bottom and top of a control volume (see Figure 3).
u_w	Tangential component of velocity induced at the cylinder by the free vorticity in the fluid.
U_∞	Onset flow velocity.
$\mathbf{V}_p$	Velocity induced at an arbitrary point p.
γ	Bound vorticity on cylinder surface.
η	Body orientated co-ordinate which increases in the radial direction.
θ, ϕ	Angles identifying points on cylinder surface. Measured counter-clockwise from rear stagnation point.
ν	Kinematic viscosity.
ξ	Body orientated co-ordinate which increases clockwise in the tangential direction.
ω	Free vorticity.

Subscripts and superscripts

n	Summation index.
0	Arbitrary point in flow field associated with free vorticity.

p Arbitrary point in flow field.
s Arbitrary point on cylinder surface associated with bound vorticity.

REFERENCES

1. Ta Phuoc Loc, 'Numerical analysis of unsteady secondary vortices generated by an impulsively started circular cylinder', *J. Fluid Mechanics*, **100**, 111–128 (1980).
2. M. E. Taslim, R. B. Kinney and M. A. Paolino, 'Analysis of two-dimensional viscous flow over cylinders in unsteady motion', *AIAA Journal*, **22**, 586–594 (1984).
3. H. Hasimoto, 'On the periodic fundamental solutions of the Stokes equations and their application to viscous flow past a cubic array of spheres', *J. Fluid Mechanics*, **5**, 317–328 (1959).
4. J. Happel, 'Viscous flow relative to arrays of cylinders', *American Institute of Chemical Engineering Journal*, **5**, 174–177 (1959).
5. A. Umemura, 'Matched-asymptotic analysis of low-Reynolds-number flow past two equal circular cylinders', *J. Fluid Mechanics*, **121**, 345–363 (1982).
6. H. Yano and A. Kieda, 'An approximate method for solving two-dimensional low-Reynolds-number flow past arbitrary cylindrical bodies', *J. Fluid Mechanics*, **97**, 157–179 (1980).
7. M. Kiya, M. Arie, H. Tamura and H. Mori, 'Vortex shedding from two circular cylinders in staggered arrangement', *J. Fluids Engineering*, **102**, 166–173 (1980).
8. D. Gordon, 'Numerical calculations on viscous flow fields through cylinder arrays', *Computers and Fluids*, **6**, 1–13 (1978).
9. R. A. Schmall, and R. B. Kinney, 'Numerical study of unsteady viscous flow past a lifting plate', *AIAA Journal*, **12**, 1566–1573 (1974).
10. R. B. Kinney, and Z. M. Cielak, 'Analysis of unsteady viscous flow past an airfoil: part I—theoretical development', *AIAA Journal*, **15**, 1712–1717 (1977).
11. Z. M. Cielak and R. B. Kinney, 'Analysis of unsteady viscous flow past an airfoil: part II—numerical formulation and results', *AIAA Journal*, **16**, 105–110 (1978).
12. J. C. Wu, 'Fundamental solutions and numerical methods for flow problems', *Int. j. numer. methods fluids*, **4**, 185–201 (1984).
13. L. M. Milne-Thomson, *Theoretical Hydrodynamics*, 4th edn, MacMillan, London, 1966.
14. E. A. Cerutti, 'Numerical predictions for unsteady viscous flow past an array of cylinders', *Ph.D. Dissertation*, University of Arizona, 1984.
15. F. C. Thames, 'Numerical solution of the incompressible Navier-Stokes equations about arbitrary two-dimensional bodies', *Ph.D. Dissertation*, Mississippi State University, Mississippi, 1975.
16. D. C. Thoman and A. A. Szewczyk, 'Time-dependent viscous flow over a circular cylinder', *Physics of Fluids*, Suppl. II, 76–86 (1969).
17. S. K. Jordan and J. E. Fromm, 'Oscillatory drag, lift and torque on a circular cylinder in a uniform flow', *Physics of Fluids*, **15**, 371–376 (1972).
18. A. J. Chorin, 'Numerical study of slightly viscous flow', *J. Fluid Mechanics*, **57**, 785–796 (1973).
19. W. M. Collins and S. C. R. Dennis, 'Flow past an impulsively started cylinder', *J. Fluid Mechanics*, **60**, 105–127 (1973).
20. B. Fornberg 'A numerical study of steady viscous flow past a circular cylinder', *J. Fluid Mechanics*, **98**, 819–855 (1980).
21. S. J. Cowley 'Computer extension and analytical continuation of Blasius' expansion for impulsive flow past a circular cylinder', *J. Fluid Mechanics*, **135**, 389–405 (1983).